# Weak Lensing Predictions at Intermediate Scales

Ludovic Van Waerbeke[1,2], Takashi Hamana[2], Román Scoccimarro[3],
Stephane Colombi[2,4], Francis Bernardeau[5]

[1] *Canadian Institute for Theoretical Astrophysics, 60 St George Str., Toronto, M5S 3H8, Canada*
[2] *Institut d'Astrophysique de Paris, 98*[bis] *Bld Arago, 75014 Paris, France*
[3] *Institute for Advanced Study, Einstein Drive, Princeton, NJ 08540, United States*
[4] *Numerical Investigations in Cosmology (N.I.C.), CNRS, France*
[5] *Service de Physique Théorique. C.E. de Saclay. 91191 Gif sur Yvette Cedex, France*

24 October 2018

**ABSTRACT**

As pointed out in previous studies, the measurement of the skewness of the convergence field $\kappa$ will be useful in breaking the degeneracy among the cosmological parameters constrained from weak lensing observations. The combination of shot noise and finite survey volume implies that such a measurement is likely to be done in a range of intermediate scales ($0.5'$ to $20'$) where neither perturbation theory nor the hierarchical ansatz apply. Here we explore the behavior of the skewness of $\kappa$ at these intermediate scales, based on results for the non-linear evolution of the mass bispectrum. We combined different ray-tracing simulations to test our predictions, and we find that our calculations describe accurately the transition from the weakly non-linear to the strongly non-linear regime. We show that the single lens-plane approximation remains accurate even in the non-linear regime, and we explicitly calculate the corrections to this approximation. We also discuss the prospects of measuring the skewness in upcoming weak lensing surveys.

**Key words:** cosmology: gravitational lensing, large-scale structure of the universe

## 1 INTRODUCTION

Weak lensing by large scale structures has been recognized for a decade as a potentially powerful tool to probe the distribution of dark matter in the Universe, as well as a way to measure the cosmological parameters ((Blandford et al. 1991; Miralda-Escude 1991; Kaiser 1992; Villumsen 1996; Bernardeau, Van Waerbeke & Mellier 1997; Jain & Seljak 1997; Schneider et al. 1998)). Reports of sound detections of such an effect have been done recently by different groups ((Van Waerbeke et al. 2000; Wittman et al. 2000; Bacon, Refregier & Ellis 2000; Kaiser, Wilson & Luppino 2000)) from independent data sets and data analysis procedures. These first measurements are detections of the excess variance of galaxy ellipticities with respect to a random orientation of the intrinsic ellipticities, and are in very good agreement with theoretical expectations based on cluster normalized models of structure formation. These detections demonstrate that the systematic errors can be controlled down to a low enough level; this is a remarkable achievement that paves the way to genuine reconstruction of projected mass maps of the Universe.

The aim of projected mass maps is not only to measure the projected mass power spectrum. It has indeed been stressed that valuable constraints on cosmological parameters are expected to come from a joint measurement of variance and higher order moments such as the skewness of the convergence ((Bernardeau, Van Waerbeke & Mellier 1997; Jain & Seljak 1997; Schneider et al. 1998; Van Waerbeke, Bernardeau, Mellier, 1999)). This is because the variance is strongly dependent on both the amplitude of the mass power spectrum and the density of the Universe, while the skewness (properly normalized) is essentially a measure of the latter. Another motivation for measuring the skewness of the convergence comes from recent works on the possible existence of intrinsic correlations in the galaxy ellipticities ((Heavens, Refregier & Heymans 2000; Croft & Metzler 2000; Catelan, Kamionkowski & Blandford 2000)). This might indeed challenge the cosmological interpretation of weak lensing surveys if part of the signal is due to intrinsic alignment of galaxies. However, additional information on the statistics of the signal such as the skewness can provide a way to confirm the nature of it (e.g. a signal dominated by intrinsic ellipticity alignments may not lead to a measurable skewness as pointed out in (Croft & Metzler 2000)).

Current skewness predictions rely mostly on perturbative analysis of structure growth which is expected to break down at scales (around a few arcmins) where the lensing

signal is easier to measure. It is therefore desirable to dispose also of intermediate and small scale predictions for the higher order moments. For the second moment, the variance, the nonlinear evolution of the power spectrum have been used since the early calculations ((Miralda-Escude 1991; Jain & Seljak 1997; Schneider et al. 1998)). These calculations are based on a fitting formula for the non-linear evolution of the mass power spectrum ((Hamilton et al. 1991; Peacock & Dodds 1996)) accurate to $\sim 15\%$, depending on the cosmological model. (Jain & Seljak 1997) and (Schneider et al. 1998) used this phenomenological approach to compute the non-linear convergence power spectrum, the small-scale shear variance and its correlation functions. The results are in remarkably good agreement with ray-tracing simulations ((Jain, Seljak & White 2000)). Unfortunately the non-linear evolution of higher order statistics cannot be simply described by the non-linear power spectrum alone because a description of the non-linear evolution of mode coupling is also required. For instance, the non-linear evolution of the skewness directly depends on how the bispectrum evolves.

Prescriptions for the non-linear evolution of the bispectrum were not available until very recently. Such an issue is obviously closely related to the understanding of the non-linear gravitational dynamics that has been extensively studied for the last 10 years. Although these efforts were primarily done for studying the galaxy clustering properties one can take advantage of the results that have emerged in this domain. Recently, Hui (1999) extended the skewness calculations in the strongly non-linear regime using "hyper-extended perturbation theory" (hereafter HEPT, (Scoccimarro & Frieman 1999)). The predictions agree well with ray tracing simulations ((Jain, Seljak & White 2000)) at very small scales $(0.1')$, but overestimate the simulation values at larger scales. This is expected since HEPT was proposed to work in the non-linear regime, where the hierarchical clustering ansatz is assumed to hold. Extensions of this approach presented in the literature ((Valageas 2000; Munshi & Coles 2000; Munshi & Jain 2000a; Munshi & Jain 2000b) and (Bernardeau & Valageas 2000)) are also based on the hierarchical ansatz, and thus suffer from the same limitations. Recently, Scoccimarro & Couchman (2000) obtained a fitting formula for the bispectrum based on numerical simulations of CDM models. In this paper, we use this result to compute the skewness of the convergence $\kappa$ and compare it to ray-tracing simulations. This allows to bridge the gap between previous results restricted to either the non-linear regime or the weakly non-linear regime where perturbation theory holds. A different approach to this problem, using Press-Schechter halos, is given by Cooray & Hu (2000).

Taking advantage of these investigations, we also address the importance of the lens-lens coupling effects and of the Born approximation, which are routinely used in weak lensing calculations. It is usually assumed (see (Bernardeau, Van Waerbeke & Mellier 1997)) in semi-analytical predictions that the coupling between lens planes is negligible, as well as the successive deflections of the lensed light ray. This is equivalent to assume that the Universe can be approximated by a single lens plane at some *fiducial* redshift. There is *a priori* no reason to believe that these approximations are still valid in the non-linear regime. Here we test quantitatively these approximations down to very small scales both using our ray-tracing simulations and semianalytic predictions.

The questions we address in this paper are therefore the following: does the non-linear prediction of the skewness $S_3(\kappa)$ based on the non-linear evolution of the bispectrum describe correctly intermediate scales? Is the skewness of the convergence still an efficient way of discriminating between different cosmologies? Are the corrections to the unperturbed ray-path given by the Born approximation and lens-lens coupling terms still negligible at non-linear scales?

The paper is organized as follows. Basic definitions, perturbative expressions and the description of the non-linear bispectrum are reviewed in Section 2. In Section 3, we give the relevant equations to calculate the variance and the skewness of the convergence, including correction terms due to lens-lens couplings and deviations from the Born approximation. Section 4 describes the ray-tracing simulations. We present our results in Section 5 and conclusions in Section 6.

## 2 DENSITY FIELD STATISTICS

### 2.1 Perturbative Regime

We assume the standard model of structure growth from initial Gaussian fluctuations. Perturbation theory ((Peebles 1980; Fry 1984)) which describes the evolution of the density contrast $\delta(\mathbf{x}, t) = (\rho(\mathbf{x}, t) - \bar{\rho}(t))/\bar{\rho}(t)$ is well known, therefore we shall quote here only the results and notations needed in this paper. The Fourier transform $\tilde{\delta}(\mathbf{k}, t)$ of the density contrast is defined as

$$\tilde{\delta}(\mathbf{k}, t) = \int \frac{\mathrm{d}^3 \mathbf{x}}{(2\pi)^3} \delta(\mathbf{x}, t) \, e^{-i\mathbf{k}\cdot\mathbf{x}}. \tag{1}$$

If $\delta \ll 1$ (perturbative regime), for an Einstein-de Sitter Universe $(\Omega_0 = 1, \Lambda = 0)$, the solution of the equation of motion of $\delta$ can be written as the following perturbation expansion

$$\tilde{\delta}(\mathbf{k}, t) = \sum_{i=1}^{\infty} a^i(t)\tilde{\delta}^{(i)}(\mathbf{k}), \tag{2}$$

where $a(t)$ is the scale factor such that $a(t_0) = 1$ today. For $\Omega \neq 1$ the time dependence can still be factorized to a very good accuracy (see eg. (Bouchet et al. 1992) for full second-order results) although the growth factor is a more complicated function of time than $a(t)$. At any order, the $\tilde{\delta}^{(i)}(\mathbf{k})$'s can be expressed in terms of the first order fluctuation $\tilde{\delta}^{(1)}(\mathbf{k})$ (Goroff et al. 1986)

$$
\begin{aligned}
\tilde{\delta}^{(i)}(\mathbf{k}) \ = \ & \int \mathrm{d}^3\mathbf{k}_1 ... \int \mathrm{d}^3\mathbf{k}_i \; \delta_D(\mathbf{k} - \mathbf{k}_1 - ... - \mathbf{k}_i) \times \\
& F_i(\mathbf{k}_1, ..., \mathbf{k}_i)\tilde{\delta}^{(1)}(\mathbf{k}_1)...\tilde{\delta}^{(1)}(\mathbf{k}_i),
\end{aligned} \tag{3}
$$

where the kernels $F_i(\mathbf{k}_1, ..., \mathbf{k}_i)$ are non-linear scalar functions of the wave vectors $\mathbf{k}_1, ..., \mathbf{k}_i$. The power spectrum $P(k)$ and the bispectrum $B(\mathbf{k}_1, \mathbf{k}_2, \mathbf{k}_3)$ are defined as

$$
\begin{aligned}
\langle \tilde{\delta}(\mathbf{k}_1)\tilde{\delta}(\mathbf{k}_2) \rangle \ &= \ \delta_D(\mathbf{k}_1 + \mathbf{k}_2) \; P(k) \\
\langle \tilde{\delta}(\mathbf{k}_1)\tilde{\delta}(\mathbf{k}_2)\tilde{\delta}(\mathbf{k}_3) \rangle \ &= \ \delta_D(\mathbf{k}_1 + \mathbf{k}_2 + \mathbf{k}_3) \; B(\mathbf{k}_1, \mathbf{k}_2, \mathbf{k}_3).
\end{aligned} \tag{4}
$$

Incorporating Eq.(3) into Eq.(4) leads to the expression of the bispectrum as a function of the second-order kernel $F_2(\mathbf{k}_1, \mathbf{k}_2)$ and the power spectrum

$$
\begin{aligned}
B(\mathbf{k}_1, \mathbf{k}_2, \mathbf{k}_3) &= 2\, F_2(\mathbf{k}_1, \mathbf{k}_2)\, P(k_1)P(k_2) \\
&+ 2\, F_2(\mathbf{k}_2, \mathbf{k}_3)\, P(k_2)P(k_3) \\
&+ 2\, F_2(\mathbf{k}_1, \mathbf{k}_3)\, P(k_1)P(k_3),
\end{aligned} \tag{5}
$$

where ((Fry 1984))

$$
F_2(\mathbf{k}_1, \mathbf{k}_2) = \frac{5}{7} + \frac{1}{2}\frac{\mathbf{k}_1 \cdot \mathbf{k}_2}{k_1 k_2}\left(\frac{k_1}{k_2} + \frac{k_2}{k_1}\right) + \frac{2}{7}\left(\frac{\mathbf{k}_1 \cdot \mathbf{k}_2}{k_1 k_2}\right)^2. \tag{6}
$$

Note that Eq.(4) implies that the bispectrum is defined only for closed triangles formed by the wave vectors $\mathbf{k}_1, \mathbf{k}_2, \mathbf{k}_3$.

## 2.2 Non-Linear Power Spectrum and Bispectrum

The non-linear prediction of the skewness requires two ingredients: the non-linear evolution of the power spectrum and bispectrum. To describe the non-linear power spectrum, we use the fitting formula of ((Peacock & Dodds 1996)), based on early work by ((Hamilton et al. 1991)), and obtained by fitting the non-linear power spectrum in numerical simulations.

In order to describe the bispectrum at all scales, we use the fitting formula derived by Scoccimarro & Couchman (2000) for the non-linear evolution of the bispectrum in numerical simulations of CDM models, extending previous work for scale-free initial conditions ((Scoccimarro & Frieman 1999)). The kernel $F_2(\mathbf{k}_1, \mathbf{k}_2)$ in Eq.(5) is simply replaced by an *effective* kernel $F_2^{\mathrm{eff}}(\mathbf{k}_1, \mathbf{k}_2)$ such that

$$
\begin{aligned}
F_2^{\mathrm{eff}}(\mathbf{k}_1, \mathbf{k}_2) &= \frac{5}{7}\, a(n, k_1)a(n, k_2) \\
&+ \frac{1}{2}\frac{\mathbf{k}_1 \cdot \mathbf{k}_2}{k_1 k_2}\left(\frac{k_1}{k_2}\frac{k_2}{k_1}\right)\, b(n, k_1)b(n, k_2) \\
&+ \frac{2}{7}\left(\frac{\mathbf{k}_1 \cdot \mathbf{k}_2}{k_1 k_2}\right)^2\, c(n, k_1)c(n, k_2),
\end{aligned} \tag{7}
$$

with

$$
\begin{aligned}
a(n, k) &= \frac{1 + \sigma_8^{-0.2}(z)\,[0.7\, Q_3(n)]^{1/2}\,(q/4)^{n+3.5}}{1 + (q/4)^{n+3.5}} \\
b(n, k) &= \frac{1 + 0.4\,(n+3)\, q^{n+3}}{1 + q^{n+3.5}} \\
c(n, k) &= \frac{1 + 4.5/\left[1.5 + (n+3)^4\right]\,(2q)^{n+3}}{1 + (2q)^{n+3.5}},
\end{aligned} \tag{8}
$$

and $q \equiv k/k_{NL}(z)$, where $4\pi k_{NL}^3 P_L(k_{NL}) = 1$, and $P_L(k)$ is the linear power spectrum at the desired redshift. The effective spectral index is taken from the linear power spectrum as well. The function $Q_3(n)$ is given by

$$
Q_3(n) = \frac{(4 - 2^n)}{(1 + 2^{n+1})}, \tag{9}
$$

which is the "saturation value" obtained in HEPT ((Scoccimarro & Frieman 1999)). From these expressions, it follows that at large scales, where the functions $a = b = c = 1$, we recover the tree-level PT. On the other hand, at small scales, where $a^2 = (7/10)Q_3(n)\sigma_8^{-0.4}$ and $b = c = 0$ the bispectrum becomes hierarchical with an amplitude that approximately

reproduces HEPT for $\sigma_8 \approx 1$. For more details see Scoccimarro & Couchman (2000).

## 3 GRAVITATIONAL LENSING STATISTICS

Calculations of gravitational lensing statistics using perturbation theory have been presented in detail in the literature (e.g. see (Bernardeau, Van Waerbeke & Mellier 1997)). Therefore, we give without derivation the expressions of the second and third moments of the convergence field $\kappa$ as well as the skewness correction terms due to lens-lens coupling and deviations from the Born approximation.

### 3.1 Basics of Gravitational Lensing

We use notations similar to (Schneider et al. 1998) with $c = H_0 = 1$, since the results do not depend on the Hubble constant. In a FRW Universe with a matter density $\Omega_0$ and cosmological constant $\Lambda$, the radial distance $w(z)$ and the angular diameter distance $f_K(z)$ are defined as

$$
w(z) = \int_0^z \frac{\mathrm{d}z}{\sqrt{(1+z')^3\Omega_0 + (1+z')^2(1 - \Omega_0 - \Omega_\Lambda) + \Omega_\Lambda}} \tag{10}
$$

$$
f_K(w) = \begin{cases} \Omega_K^{-1/2} \sin\sqrt{\Omega_K}w & \text{for } \Omega_K > 0 \\ w & \text{for } \Omega_K = 0 \\ |\Omega_K|^{-1/2} \sinh\sqrt{|\Omega_K|}w & \text{for } \Omega_K < 0. \end{cases} \tag{11}
$$

where $\Omega_K = \Omega_0 + \Omega_\Lambda - 1$ is the curvature. In the absence of lensing, the comoving angular distance $\mathbf{x}(\boldsymbol{\theta}, w)$ at a radial distance $w(z)$ between a light ray in the direction $\boldsymbol{\theta}$ and a fiducial light ray is $\mathbf{x}(\boldsymbol{\theta}, w) = \boldsymbol{\theta} f_K(w)$. In the presence of density fluctuations, a light ray experiences many deflections such that $\mathbf{x}(\boldsymbol{\theta}, w)$ becomes

$$
\mathbf{x}(\boldsymbol{\theta}, w) = \boldsymbol{\theta} f_K(w) - 2\int_0^w \mathrm{d}w'\, f_K(w - w')\nabla_\perp \Phi\left[\mathbf{x}(\boldsymbol{\theta}, w'), w'\right], \tag{12}
$$

where $\Phi$ is the 3-dimensional gravitational potential. The gradient $\nabla_\perp$ denotes the derivatives with respect to $\mathbf{x}$ in the plane perpendicular to the line-of-sight at distance $w$. The amplification matrix $\mathcal{A}(\boldsymbol{\theta}, w)$ describes the mapping between the source plane at $w(z)$

$$
\mathcal{A}(\boldsymbol{\theta}, w) = \frac{1}{f_K(w)}\frac{\partial \mathbf{x}}{\partial \boldsymbol{\theta}}, \tag{13}
$$

which using the first order expansion of Eq.(12) becomes $\mathcal{A}_{ij} \simeq \delta_{ij}^K + \Psi_{ij}$ with

$$
\begin{aligned}
\Psi_{ij}(\boldsymbol{\theta}, w) &= -2\int_0^w \mathrm{d}w'\frac{f_K(w - w')\, f_K(w')}{f_K(w)} \times \\
&\quad \Phi_{,ij}^{(1)}\left(f_K(w')\boldsymbol{\theta}, w'\right).
\end{aligned} \tag{14}
$$

The convergence $\kappa$ and the shear $\boldsymbol{\gamma}$ are defined such that the amplification matrix takes the symmetric form

$$
\mathcal{A}(\boldsymbol{\theta}, w) = \begin{pmatrix} 1 - \kappa - \gamma_1 & -\gamma_2 \\ -\gamma_2 & 1 - \kappa + \gamma_1 \end{pmatrix}, \tag{15}
$$

$\kappa$ and $\boldsymbol{\gamma}$ are therefore line-of-sight integrals from the source distance $w(z)$ to 0. If the sources are distributed in redshift according to some function $p_s(w)$, the convergence $\kappa$ can still be expressed as a simple line-of-sight integral

$$\kappa(\boldsymbol{\theta}) = \frac{3}{2}\Omega_0 \int_0^{w_H} \mathrm{d}w \frac{g(w)}{a(w)} f_K(w)\, \delta(f_K(w)\boldsymbol{\theta}, w), \qquad (16)$$

where

$$g(w) = \int_w^{w_H} \mathrm{d}w'\, p_s(w')\, \frac{f_K(w - w')}{f_K(w')}, \qquad (17)$$

and $w_H$ is the radial distance to the horizon.

## 3.2 Variance and Skewness of the Smoothed Convergence

In perturbation theory, the moments are calculated from a perturbative expansion of the density contrast. The $i^{\mathrm{th}}$ order of the convergence field is therefore

$$\kappa^{(i)}(\boldsymbol{\theta}) = \frac{3}{2}\Omega_0 \int_0^{w_H} \mathrm{d}w \frac{g(w)}{a(w)} f_K(w)\, \delta^{(i)}(f_K(w)\boldsymbol{\theta}, w). \quad (18)$$

The calculation of the smoothed second and third moments is then straightforward. The leading order contributions to these moments are $\langle \kappa^2 \rangle_{\theta_0} = \langle \kappa^{(1)^2} \rangle_{\theta_0}$ and $\langle \kappa^3 \rangle_{\theta_0} = 3\langle \kappa^{(1)^2} \kappa^{(2)} \rangle_{\theta_0}$ respectively. Let us call $I(k)$ the Fourier transform of the smoothing window and define the angular wave vector $\mathbf{s} = f_K(w)\mathbf{k}_\perp$. As calculated in (Bernardeau, Van Waerbeke & Mellier 1997) and (Schneider et al. 1998) the second moment is

$$\begin{aligned}\langle \kappa^2 \rangle_{\theta_0} &= 2\pi \frac{9}{4}\Omega_0^2 \int_0^{w_H} \mathrm{d}w\, \frac{g^2(w)}{a^2(w)} \times \\ &\int_0^\infty s \mathrm{d}s\, P\left(\frac{s}{f_K(w)}, w\right) [I(s\theta_0)]^2, \end{aligned} \qquad (19)$$

and the third moment

$$\begin{aligned}\langle \kappa^3 \rangle_{\theta_0} &= \frac{1}{2\pi}\frac{81}{4}\Omega_0^3 \int_0^{w_H} \mathrm{d}w\, \frac{g^3(w)}{a^3(w)f_K(w)} \times \\ &\int_0^\infty \mathrm{d}^2\mathbf{s}_1\, P\left(\frac{s_1}{f_K(w)}, w\right)\, I(s_1\theta_0) \times \\ &\int_0^\infty \mathrm{d}^2\mathbf{s}_2\, P\left(\frac{s_2}{f_K(w)}, w\right)\, I(s_2\theta_0) \times \\ &I(|\mathbf{s}_1 + \mathbf{s}_2|\theta_0)\, F_2(\mathbf{s}_1, \mathbf{s}_2). \end{aligned} \qquad (20)$$

These expressions rely on the validity of Eq.(14) which involves two approximations: one is that we assume the light rays travel along the unperturbed light paths (the so-called Born approximation), and the second is that we neglect non-linear terms in the amplification matrix (which is physically equivalent to neglecting all the couplings between subsequent lenses). These two approximations ignore quadratic terms of the form $\kappa \cdot \kappa$, $\kappa \cdot \gamma$ or $\gamma \cdot \gamma$ (see (Bernardeau, Van Waerbeke & Mellier 1997)). There is no reason a priori to neglect these terms in the skewness calculation, because they give a contribution of the same order as Eq.(20). We shall address this question in the next Section.

## 3.3 Skewness Corrections due to Lens-Lens Couplings and Deviations from Born Approximation

The effect of dropping the lens-lens coupling and the Born approximation has been calculated in the weakly non-linear

regime (see (Bernardeau, Van Waerbeke & Mellier 1997) and (Schneider et al. 1998)). The contribution to the skewness can be calculated by considering the perturbation expansion up to the second order in the gravitational potential in Eq.(13), which leads to a second order correction term $\mathcal{A}_{ij}^{(2)}$ in Eq.(14). After lengthy but straightforward calculations, the correction to the third moment $\langle \kappa^3 \rangle_{\theta_0}^{\mathrm{corr}}$ can be derived:

$$\begin{aligned}\langle \kappa^3 \rangle_{\theta_0}^{\mathrm{corr}} &= \frac{243}{8\pi}\Omega_o^4 \int_0^{w_H} \mathrm{d}w \frac{g^2(w)}{a^2(w)} \int_0^w \mathrm{d}w' \frac{g(w')}{a^2(w')}\frac{f_K(w - w')}{f_K(w)} \times \\ &\int \mathrm{d}^2\mathbf{s}_1\, P\left(\frac{s_1}{f_K(w)}, w\right)\, I(s_1\theta) \times \\ &\int \mathrm{d}^2\mathbf{s}_2\, P\left(\frac{s_2}{f_K(w')}, w'\right)\, I(s_2\theta) \times \\ &I(|\mathbf{s}_1 + \mathbf{s}_2|\theta) \left[\left(\frac{\mathbf{s}_1 \cdot \mathbf{s}_2}{s_1 s_2}\right)^2 + \frac{\mathbf{s}_1 \cdot \mathbf{s}_2}{s_2}\right]. \end{aligned} \qquad (21)$$

The similarity with Eq.(20) is quite obvious, which shows that the two terms ($\langle \kappa^3 \rangle_{\theta_0}$ and $\langle \kappa^3 \rangle_{\theta_0}^{\mathrm{corr}}$) are of the same order $\delta^{(1)^4}$ in the perturbative sense. The only difference between the two expressions lies in the double time integral here. It was shown ((Bernardeau, Van Waerbeke & Mellier 1997) and (Schneider et al. 1998)) that this double integral makes the correction term Eq.(21) only a few percent of Eq.(20). In other words, even though the two expressions have indeed the same order $\propto \delta^{(1)^4}$, they differ by almost one order of magnitude just because of the additional $f_K(w - w')/f_K(w)$ factor in Eq.(21) (in the case of a single source redshift this factor is equivalent to an additional $g(w)$ factor, according to Eq.(17)). It is therefore correct to say that the lensing efficiency function $g(w)$ can play the role of a perturbative parameter as the density contrast does (when $\delta \ll 1$). The smallness of $\langle \kappa^3 \rangle_{\theta_0}^{\mathrm{corr}}$ shows that even in the weakly non-linear regime, terms involving powers of $g(w)$ higher than 1 will always be small compared to terms only proportional to $g(w)$. In the following we shall compute Eq.(21) in the non-linear regime, and use results from ray-tracing simulations in order to check if this statement is still valid when the density contrast is much larger than 1.

## 3.4 Calculations and Filtering Schemes

We can now calculate the variance, the skewness and its correction of the convergence field using the Eq.(19), (20) and (21) by forming the ratios:

$$S_3(\kappa) = \frac{\langle \kappa^3 \rangle_{\theta_0}}{\langle \kappa^2 \rangle_{\theta_0}^2} \quad ; \quad \Delta S_3(\kappa) = \frac{\langle \kappa^3 \rangle_{\theta_0}^{\mathrm{corr}}}{\langle \kappa^2 \rangle_{\theta_0}^2} \qquad (22)$$

It is worth to notice that $\Delta S_3(\kappa)$ is weakly dependent on the cosmological parameters since the $\Omega_0$ dependence in the front of Eq.(19) and Eq.(21) cancels out. The non-linear variance is given by Eq.(19) where the power spectrum is replaced by the Peacock & Dodds (1996) prescription as in Jain & Seljak (1997). The non-linear third moment is given by Eq.(20) where $F_2(\mathbf{k}_1, \mathbf{k}_2)$ has been replaced by $F_2^{\mathrm{eff}}(\mathbf{k}_1, \mathbf{k}_2)$ and we use the non-linear power spectrum. For the skewness correction, we only need to use the non-linear power spectrum in Eq.(21).

We use two types of filtering schemes: top-hat filtering and $M_{\rm ap}$ statistics. The Fourier transform of the top-hat window is:

$$I(\eta) = \frac{{\rm J}_1(\eta)}{\pi\eta}, \tag{23}$$

where $J$ denotes a Bessel function. The $M_{\rm ap}$ statistic can be defined either from the convergence $\kappa$ or from the tangential shear $\gamma_t$:

$$M_{\rm ap} = \int {\rm d}^2\boldsymbol{\theta}\; U(\theta)\kappa(\boldsymbol{\theta}) = \int {\rm d}^2\boldsymbol{\theta}\; Q(\theta)\gamma_t(\boldsymbol{\theta}), \tag{24}$$

where $\theta^2 Q(\theta) = 2\int_0^\theta {\rm d}\theta'\;\theta'\;U(\theta') - \theta^2 U(\theta)$, and $U(\theta)$ is the compensated filter. We use the compact compensated filter described in Schneider et al. (1998) where $U(\theta)$ is defined only for $\theta \in [0,\;\theta_0]$, and

$$U(\theta) = \frac{9}{\pi\theta_0^2}\left[1 - \left(\frac{\theta}{\theta_0}\right)^2\right]\left[\frac{1}{3} - \left(\frac{\theta}{\theta_0}\right)^2\right]. \tag{25}$$

The Fourier transform of $U(\theta)$ is

$$I(\eta) = \frac{12\;{\rm J}_4(\eta)}{\pi\eta^2}, \tag{26}$$

which is the function to be inserted in Eqs.(19, 20, 21). The motivation for using the compensated filters is illustrated on Fig.2 of Schneider et al. (1998): this filter is a pass-band filter, which is a more direct estimate of the mass band powers than the top-hat filter. Another advantage of the compensated filter is that the measurement of the skewness does not require a mass reconstruction (whereas top-hat filtered statistic does) as it can be evaluated directly from the shear (Eq.(24)). Note also that the compensated filter defined above peaks at a scale $\sim \theta_0/5$, if $\theta_0$ is the radius of the filter. Therefore at equal radius with the top-hat filter, $M_{\rm ap}$ statistics probes scales as small as $\sim \theta_0/5$.

## 4 RAY-TRACING SIMULATIONS

We use two different kind of ray-tracing simulations (high and low resolution simulations) which allow us to investigate scales from $0.1'$ to several tens of arcmins. The high resolution simulations ($0.1'$) were done by Jain, Seljak & White (2000), and are described in that paper. The investigated models in those simulations are OCDM2 and $\tau$CDM (see Table 1). The area covered by each simulation is 9 square degrees.

The numerical methods used for the low resolution simulation are basically same as those of the high resolution simulation except for a use of a tiled set of the independent particle-mesh (PM) $N$-body simulations[*]. The PM simulations use $256^2 \times 512$ particles and a force mesh of the same size in a periodic rectangular comoving box, with outputs done along the light-cone (Hamana, Colombi and Suto 2000). We performed 10, 11 and 12 independent simulations to generate the density field from $z \sim 2$ to the

[*] This code, developed by the *Numerical Investigations in Cosmology* group (*N.I.C.*), is an improved version of an earlier work by Bouchet, Adam & Pellat (1985) and by Moutarde et al. (1991), fully vectorized and optimized to run in parallel on several processors of a NEC-SX5.

**Table 1.** Ray-tracing simulations used in this work. The SCDM, OCDM1 and $\Lambda$CDM are described in Hamana et al. (in preparation) and the OCDM2 and $\tau$CDM are from Jain, Seljak & White (2000). $\theta_{res}$ indicates the angular resolution of the simulations $N_{rea}$ indicates the number of realizations per model, and Area specifies the sky coverage for each realization in square degrees. Note that the $N_{rea} = 40$ realizations are not rigorously independent, being random rotations of a single suite of simulations.

| Simulations | SCDM | OCDM1 | $\Lambda$CDM | OCDM2 | $\tau$CDM |
|---|---|---|---|---|---|
| $\Omega_0$ | 1 | 0.3 | 0.3 | 0.3 | 1 |
| $\Lambda$ | 0 | 0 | 0.7 | 0 | 0 |
| $\Gamma$ | 0.5 | 0.21 | 0.21 | 0.21 | 0.21 |
| $\sigma_8$ | 0.6 | 0.85 | 0.9 | 0.85 | 0.6 |
| $z_s$ | 1.0025 | 1.03 | 1.0034 | 1 | 1 |
| $\theta_{res}$ | 2' | 2' | 2' | 0.1' | 0.1' |
| $N_{rea}$ | 40 | 40 | 40 | 7 | 5 |
| Area | 25 | 25 | 25 | 9 | 9 |

present for SCDM, OCDM1 and $\Lambda$CDM models, respectively. We use the *tiling* technique first proposed by White & Hu (2000), i.e., the box size of each simulation is chosen so as to match to the convergence of the light ray bundle. The smallest box size is comoving $80 \times 80 \times 160 h^{-3}{\rm Mpc}^3$ for three models, while the largest box size are comoving $240 \times 240 \times 480 h^{-3}{\rm Mpc}^3$, $320 \times 320 \times 640 h^{-3}{\rm Mpc}^3$ and $400 \times 400 \times 800 h^{-3}{\rm Mpc}^3$, for SCDM, OCDM1 and $\Lambda$CDM models, respectively. These tiled sets of simulations yield a field-of-view of $5 \times 5$ square degrees.

The multiple lens-plane algorithm is used for ray-tracing as in Jain et al. (2000). The lens planes are located between $z = 0$ and $z \sim 2$ at intervals of comoving $80 h^{-1}{\rm Mpc}$. We obtained 40 realizations by randomly shifting the simulation boxes. For each realization, $512^2$ rays are traced backward from the observer's point. The initial ray directions are set on $512^2$ grids with a grid spacing of $5°/512 \sim 0.59$ arcmin. Although the results of the ray-tracing simulations (the position and amplification matrix of each rays) are stored at all lens planes, in this paper we only focus on the results at the plane closest to $z = 1$. The error bars on the results of the low resolution simulations correspond to the standard deviation among 40 realizations.

The range of filtering scales where the results of the low resolution simulation are reliable is between $4'$ and $30'$ for the statistics of the top-hat filtered convergence with source redshift $z \sim 1$. On the other hand, for the $M_{ap}$ statistics, that is between $20'$ and $100'$: the reason is that our compensated filter probes scales as small as $\sim \theta_0/5$ (see Section 3.4), therefore $M_{ap}$ predictions are likely to become inaccurate below $4' \times 5 = 20'$. The small-scale resolution limit comes from the finite spatial resolution of our PM simulations, while the large-scale limit comes from a lack of power in the density field on scales larger than the simulation box (finite size effects).

In addition to the usual *full* ray-tracing simulations, we also performed *approximated* ray-tracing which neglects both the deflection of the ray trajectory and the couplings between subsequent lenses. To be more specific, the shear tensor, $\mathbf{U}_m$ (see eq. 13 of Jain et al. 2000 for a definition), is computed on the *unperturbed* ray position, and the distor-
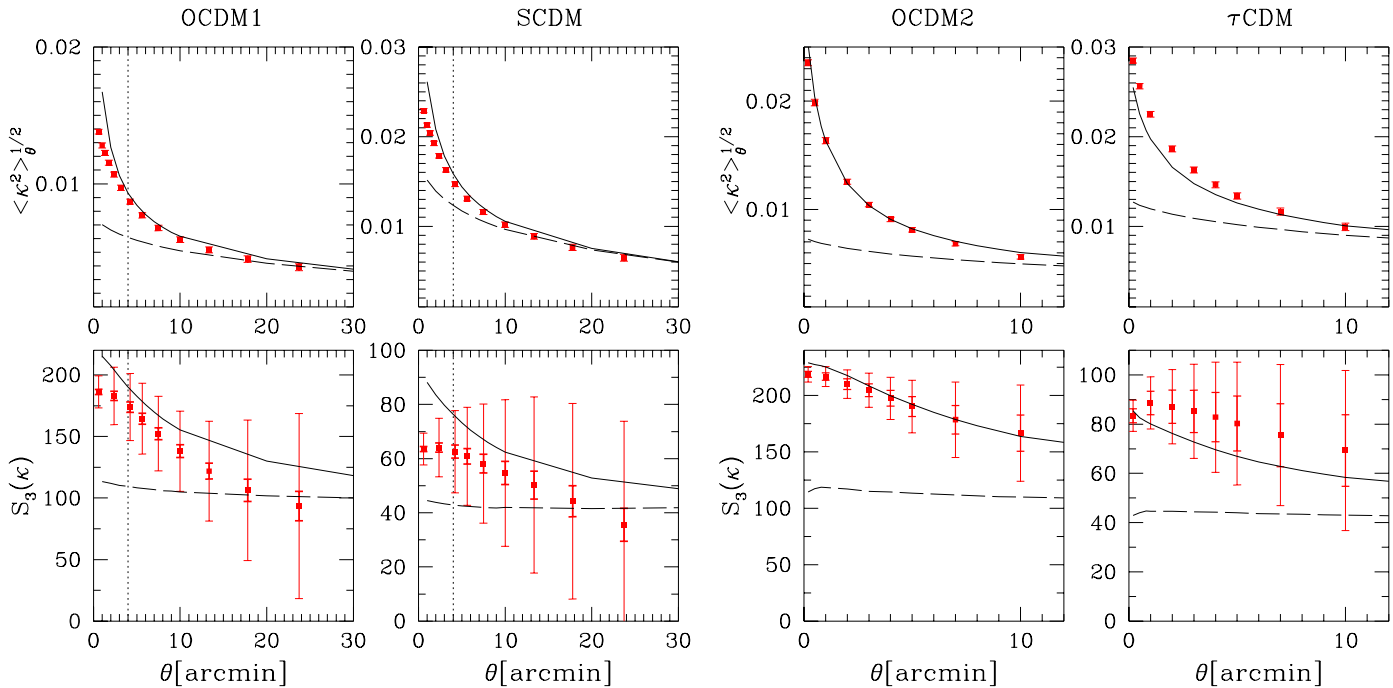
**Figure 1.** r.m.s. (top panels) and skewness (bottom panels) of the convergence field as a function of top-hat smoothing scale for the OCDM1 (far left panels) and SCDM (center-left panels) OCDM2 (center-right panels) and $\tau$CDM (far right panels) models given in Table 1. The solid line is the prediction using non-linear prescriptions for the power-spectrum and the bispectrum, and the dashed lines show the perturbation theory calculations. The vertical dotted lines in the left panels denote the reliable scale limit. The "large" error bars correspond to scaling the "small" error bars (thick lines) to a single 25 square degree (left panels) and 9 square degree (right panels) survey.

tion tensor $\mathbf{\Phi}_m$ in the right-hand-side of the eq. (14) of Jain et al. (2000) is replaced with the identity matrix to neglect all lens-lens couplings. The weak lensing statistics are then computed in the same manner as in the *full* ray-tracing case. The difference in the skewness obtained from the *full* and *approximated* simulations are computed to test the validity of the perturbative treatment in the semi-analytic predictions (§5).

## 5 RESULTS

Figures 1 and 2 show the measured r.m.s. and skewness of the convergence compared to the linear (dashed lines) and non-linear (solid lines) predictions. The square symbols represent the measurements done in the simulations. Two error bars are drawn per point: the small error bars correspond to the dispersion in the measurements taken into account all the realizations, whereas the large error bars are obtained by scaling (by $\sqrt{N_{rea}}$) the small error bars to a single realization, relevant for assesing cosmic variance in a single field of the corresponding area.

For the top-hat filtering scheme (Figure 1) the non-linear predictions give very good results for all the scales investigated (i.e. down to scales as small as $0.1'$). For the low resolution simulation (Figure 1 left panels), agreement starts to deteriorate once we reach the reliable scale limit which is $4'$ (shown by the vertical dotted lines). At smaller scales the high resolution simulations results show that the fitting formula still works down to $0.1 - 0.2'$. The agreement

starts to deteriorate quickly above the scale of $\sim 30'$ because finite field effects become important, therefore these scales are not shown here. Moreover, from a practical point of view we are less interested in these scales because residual systematics from shear measurements are supposed to dominate the lensing signal (Erben et al. 2000). The few percent discrepancy for the r.m.s. for the $\tau$CDM model (top right of Figure 1 right panels) was already observed by Jain, Seljak & White (2000), but this is consistent with the accuracy of the power spectrum fitting formula ((Peacock & Dodds 1996)). The non-linear predictions for the skewness in Fig. 1, although consistent within the errors with ray-tracing simulations, shows fluctuations of $S_3(\kappa)$ by approximately 10%. This is within the expected accuracy of the bispectrum fitting formula (15%, (Scoccimarro & Couchman 2000)); however, one must also keep in mind that this formula was obtained from single realizations of CDM models, and the bispectrum amplitude is rather sensitive to the presence of massive clusters (see Cooray & Hu 2000 for the effects of this on $S_3(\kappa)$), therefore the residual 10% fluctuation might be due to cosmic variance.

For the compensated filter (Figure 2), the difference between linear and non-linear variance is more significant, since when the spectral index becomes $n < -2$ the variance in a compensated field starts to decrease ((Schneider et al. 1998)), and this happens at much larger scales for the linear than the non-linear power spectrum. The agreement between predictions and simulations is very good for the low resolution simulations, including the skewness, and good
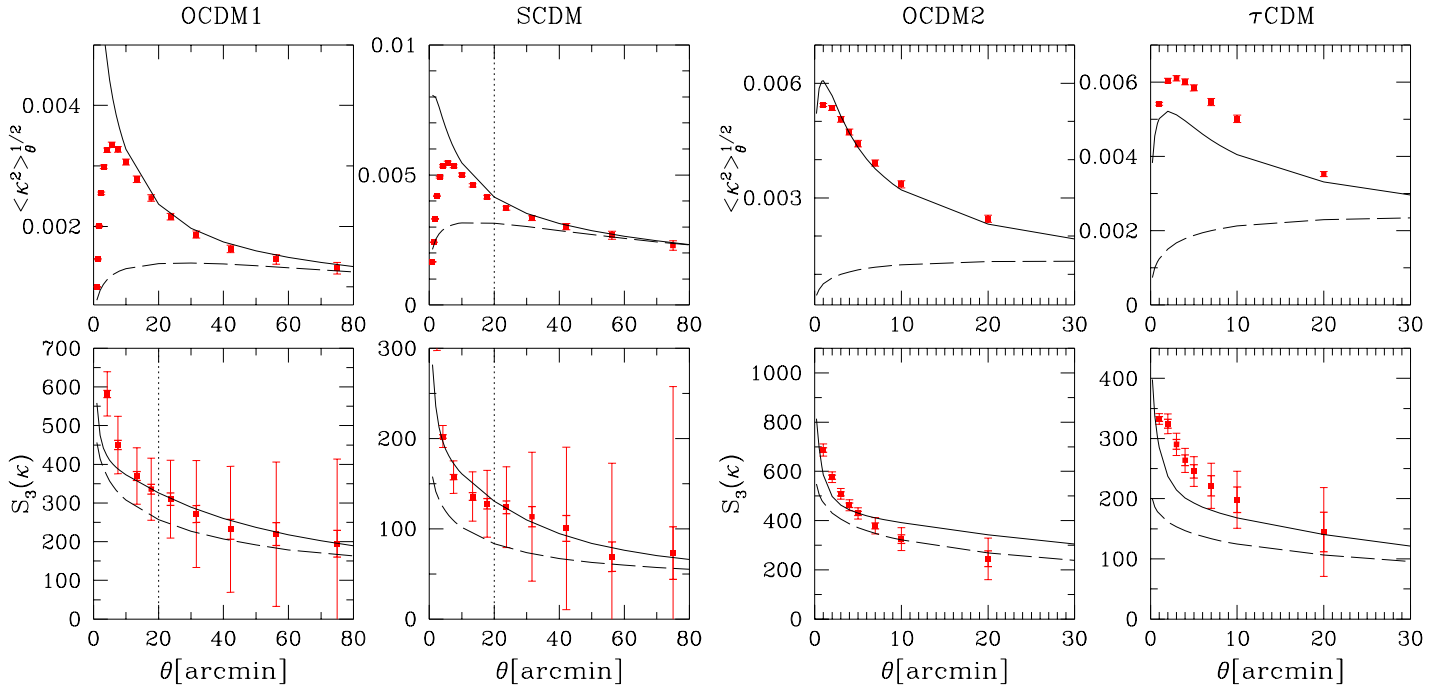
**Figure 2.** Same as Figure 1, but for the compensated filter.

for OCDM2, the high resolution case. On the other hand, the agreement is not as good for the high resolution $\tau$CDM model. The likely explanation is that the small discrepancy observed in that case for the top hat filter (Fig. 1) is amplified by the compensated filter, which acts like a derivative operator on the convergence field: as a pass-band filter, the compensated filter is more sensitive to any small discrepancy (in $k$-bands) between the non-linear power-spectrum fitting formula and the ray-tracing simulations, whereas the top-hat filter integrates over large range of $k$'s and tends to mask such discrepancies. We should note that the effects of resolution also cause the variance to decrease at small scales (top left panels in Fig. 2), therefore, at scales smaller than the resolution the agreement between the skewness prediction and the measurement in the low resolution simulation (bottom left panels in Fig. 2) is coincidental.

Figure 4 shows the skewness correction for top-hat smoothing in SCDM (top panel) and OCDM1 (bottom panel) models. The dashed line and the solid line show respectively the predictions from perturbation theory and the non-linear fitting formula, whereas points with error bars denote measurements in the ray-tracing simulations. Surprisingly, even in the non-linear regime, the correction remains small and, in fact, the relative skewness correction is smaller than in the weakly non-linear regime! As explained in Section 3.3, this means that coupling terms introduce a non-linearity which is always smaller than the non-linearity produced by very dense (non-linear) structures. In other words, even in the non-linear regime, the dominant lensing contribution comes from the single lens-plane approximation, which physically means that the probability for a given line-of-sight to pass through two very dense structures at very different resdhifts is very low. Similar results hold for the
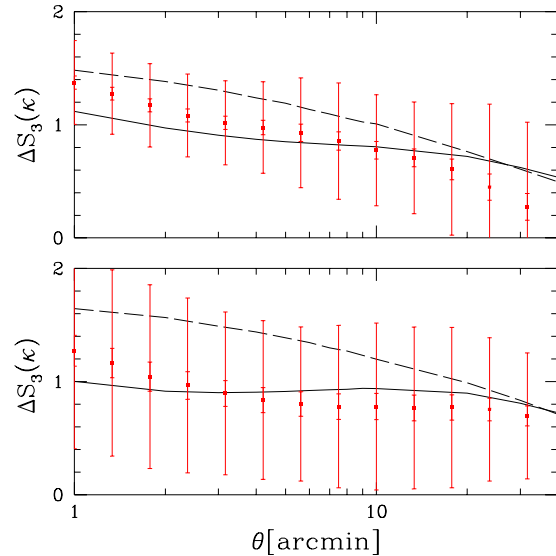


**Figure 4.** Skewness correction for top-hat smoothing $\Delta S_3(\kappa)$ as defined in Eq.(22) for the model SCDM (top panel) and OCDM1 (bottom panel). Squares with error bars correspond to measurements in the ray-tracing simulations, dashed lines to the prediction of perturbation theory, and solid lines to predictions from the non-linear fitting formula.

$M_{\rm ap}$ statistics (not shown here) where, in fact, the correction terms to the skewness are even smaller.

Figure 5 shows the predicted skewness $S_3(\kappa)$ in the $\Omega-\Lambda$ plane. Here we compare small scale (1') non-linear calculations (left panel) to larger scale (10') perturbation theory calculations (right panel) for top-hat smoothing. Note that
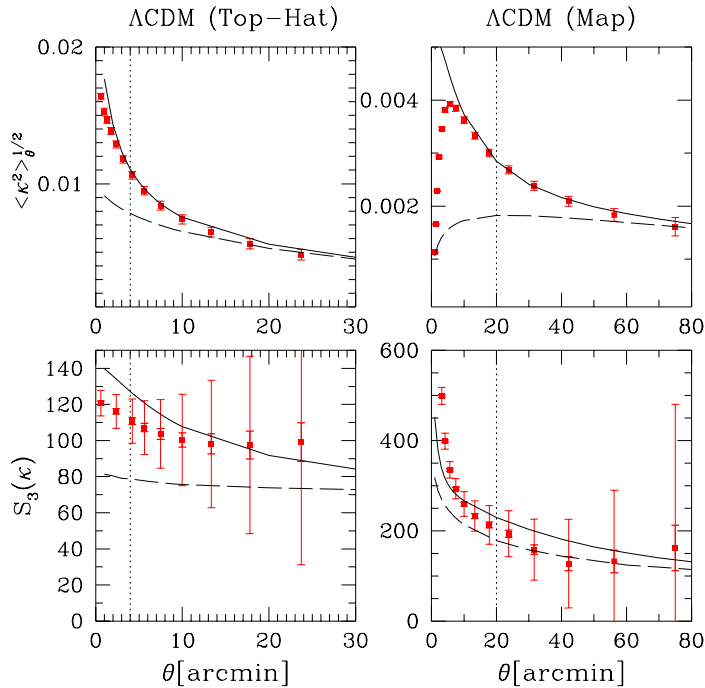
**Figure 3.** Top-hat (left panels) and compensated (right panels) statistics for the $\Lambda$CDM model (table 1).

the choice of a scale for the perturbative estimate is almost not relevant since it does depend very weakly on scale (Figure 1). This Figure shows that the cosmological dependence is preserved in the non-linear regime, and that $S_3(\kappa)$ remains essentially an estimator of $\Omega$ (the degeneracy along $\Lambda$ is strong). This result has to be compared with the Cosmic Microwave Background and the supernovae constraints, which are sensitive to the curvature and $\sim \Lambda$ respectively. This clearly motivates further lensing studies as an independent means of measuring the cosmological parameters. In fact the lensing constraints are similar to constraints derived from the galaxy catalogues or the velocity fields, although the physics is much simpler here, and weak lensing does not suffer from the galaxy bias problem.

The skewness predictions in the non-linear regime are twice their value using perturbation theory at large scales. Therefore the cosmic variance and noise analysis done in Van Waerbeke, Bernardeau & Mellier (1999) underestimated the capability of lensing surveys by a significant amount, essentially because they used very low resolution and approximate dynamics in their simulations[†]. In this work the authors shown that a 25 square degrees survey would measure the skewness at $9\sigma$, in standard observational conditions, if $\Omega = 0.3$ ($3\sigma$ if $\Omega = 1$). Here, the signal amplitude is twice larger, therefore we would need $\sim 3 - 4$ times less sky coverage to reach the same signal-to-noise ratio to measure $S_3(\kappa)$.

[†] In this work the authors used very simple lensing simulations where the mass distribution was modeled with second-order 2-dimensional lagrangian dynamics, which they had to smooth at small scale in order to avoid singularities. Because of this smoothing they obtained a skewness of the convergence close to its value in perturbation theory.

However, the exact gain depends on the precise amount of cosmic variance and shot noise at this scale. Since the cosmic variance is already given in Figure 1, we can simply add the shot noise obtained in Van Waerbeke, Bernardeau & Mellier (1999) to the high resolution simulation results presented here. It turns out that the shot noise is roughly $\sigma_{S_3} \sim 10$ at $1 - 2$ arcmin, therefore we can reach the signal-to-noise ($7 - 9\sigma$ for OCDM) with only 9 square degrees with a single measurement at $1'$. However we should keep in mind that our results for the error on the skewness in the $\Lambda$CDM model are consistent although slightly smaller than previous estimates from White & Hu (2000), possibly due to the fact that our realizations are not completely independent (being random samples of a single suite of simulations).

Finally, Fig. 6 shows the cross-correlation coefficient $r_{ij}$ between the variance measured at angular scale $\theta_i$ and $\theta_j$, for the $\Lambda$CDM model (similar results hold for the other cosmological models and for the skewness measurements as well). These results were obtained by averaging over the 40 realizations in our ensemble. The top panel presents results for the top hat filter, whereas the bottom panel corresponds to the compensated filter. We show three angular scales, $\theta_i = 5.6, 10, 23.7$ arcmin for the top hat case, and $\theta_i = 23.7, 42.2, 75$ arcmin for the compensated filter. The top hat measurements of the variance show a large cross-correlation, in fact, the cross-correlation coefficient is almost unity among all scales. On the other hand, as expected from being a band-pass filter, the compensated filter measurements are much less correlated. Note however than this result only includes cosmic variance contributions, i.e. it does not include shot noise, which can be a significant source of cross-correlations at small scales.
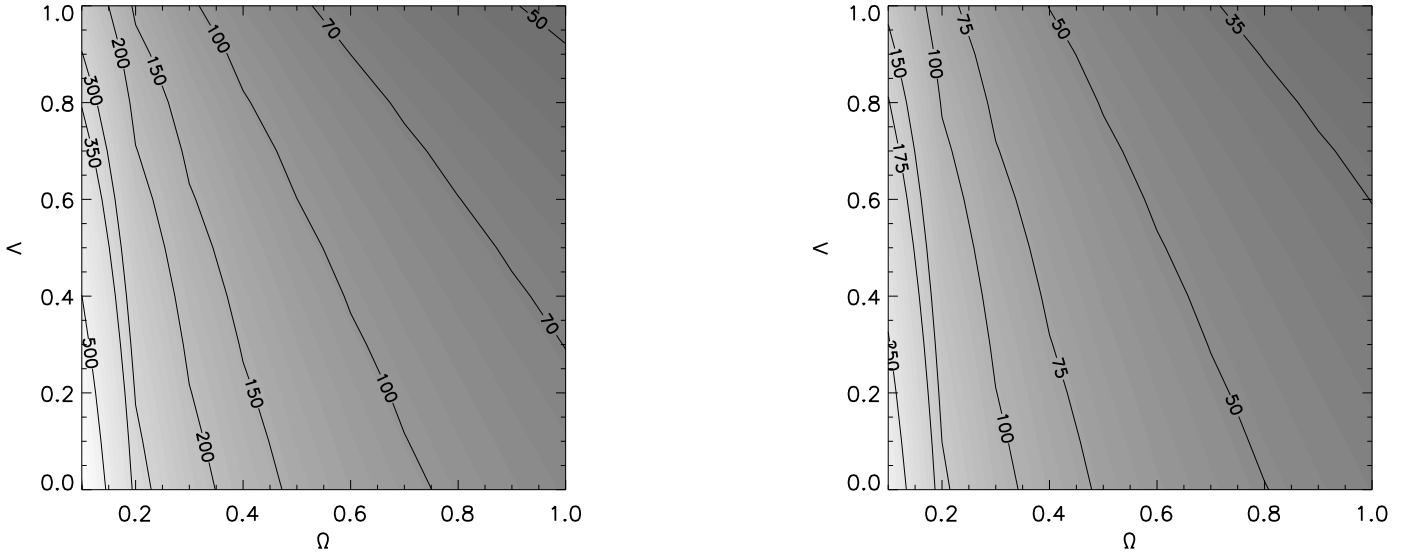
**Figure 5.** The expected skewness $S_3(\kappa)$ in the non-linear regime at a scale of $1'$ (left) compared to $S_3(\kappa)$ computed using perturbation theory at a scale of $10'$ (right) in the $\Omega$-$\Lambda$ plane. Top-Hat filtering was used. The sources are located at redshift unity. Note that for a given $\Omega$-$\Lambda$ the skewness in the left panel is roughly twice the value on the right panel.
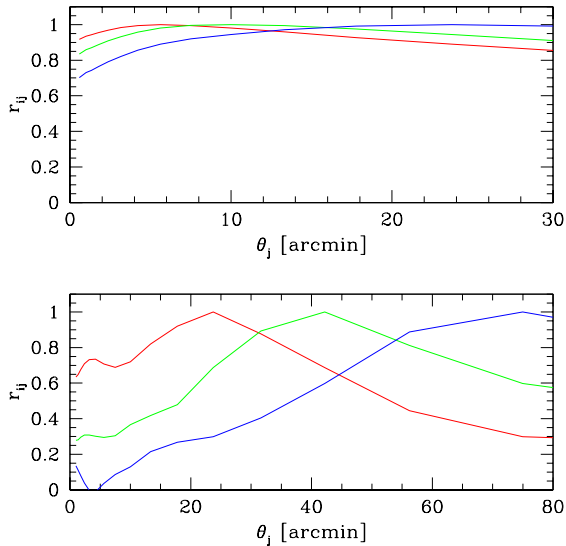


**Figure 6.** The cross-correlation coefficient $r_{ij}$ between the variance measured at angular scale $\theta_i$ and $\theta_j$, for the $\Lambda$CDM model. The top panel shows $r_{ij}$ for top-hat filtering at $\theta_i = 5.6, 10, 23.7$ arcmin as a function of $\theta_j$. The bottom panel shows $r_{ij}$ for compensated filters at $\theta_i = 23.7, 42.2, 75$ arcmin as a function of $\theta_j$.

## 6   CONCLUSIONS

We calculated semi-analytically the r.m.s. and the skewness of the convergence field $\kappa$ and showed that the non-linear prescription for the 3-dimensional bispectrum given in Scoccimarro & Couchman (2000) describes the transition from perturbative to non-linear angular scales very well with an accuracy $\sim 10\%$. We combined different ray-tracing simulations with largely different resolutions ($0.1'$ and $2'$) to compare our predictions. The transition from the weakly non-linear scales to the non-linear regime is clearly visible and also accurately described by our semi-analytical approach for both top-hat and compensated smoothing schemes for the OCDM, SCDM and $\Lambda$CDM models (The $\tau$CDM predictions are not very accurate for the compensated filter, but we suggest that it might come from innacuracies in the non-linear power spectrum fitting formula).

Our results extend previous non-linear calculations of the skewness of $\kappa$ which either assumed the validity of HEPT at all redshifts ((Hui 1999)) or relied on the hierarchical clustering ansatz ((Valageas 2000; Munshi & Coles 2000; Bernardeau & Valageas 2000)) at intermediate scales. Our semi-analytical approach allows us to investigate the cosmological dependence of the skewness of $\kappa$ in as many models as desired, without having to perform a ray tracing simulation each time.

By comparing the skewness in ray-tracing simulations with and without lens-lens coupling and Born approximation terms, we demonstrated that the single lens-plane approximation remains valid even in the highly non-linear regime, which is a non-trivial statement about weak lensing at small scales. We found that the contribution of these terms to the skewness is in remarkable agreement with the semi-analytical predictions.

We have also calculated $S_3(\kappa)$ in the $\Omega - \Lambda$ plane and shown that the signal is about twice the expected value from perturbation theory with roughly the same degeneracy in $\Lambda$ as in the perturbative case, generalizing previous results (Jain et al. 2000, White & Hu 2000). In addition, our results on the cosmic variance of the skewness suggests that a combined analysis of the existing weak lensing surveys ((Van Waerbeke et al. 2000; Wittman et al. 2000; Bacon, Refregier & Ellis 2000; Kaiser, Wilson & Luppino 2000)) should already be able to measure the skewness of the convergence.

## REFERENCES

Bacon, D., Refregier, A., Ellis, R., 2000, astro-ph/0003008

Bernardeau, F., Valageas, P., 2000, astro-ph/0006270

Bernardeau, F., Van Waerbeke, L., Mellier, Y., 1997, A&A, 322, 1

Blandford, R.D., Saust, A.B., Brainerd, T.G., Villumsen, J. V, 1991, MNRAS, 251, 600

Bouchet, F.R., Adam, J.C., Pellat, R., 1985, A&A, 144, 413

Bouchet, F.R., Juszkiewicz, R., Colombi, S., Pellat, R., 1992, ApJ, 394, L5

Catelan, P., Kamionkowski, M., Blandford, R., 2000, astro-ph/0005470

Cooray, A., Hu, W., 2000, astro-ph/0004151

Croft, R.A.C., Metzler, C., 2000, astro-ph/0005384

Erben, T., Van Waerbeke, L., Bertin, E., Mellier, Y., Schneider, P., 2000, astro-ph/0007021

Fry, J.N., 1984, ApJ, 279, 499

Goroff, M.H., Grinstein, B., Rey, S.J., Wise, M., 1986, ApJ, 311, 6

Hamana, T., Colombi, S., & Suto, Y. 2000, A&A submitted

Hamilton, A.J.S., Matthews, A., Kumar, P., Lu, E., 1991, ApJ, 274, L1

Heavens, A., Refregier, A., Heymans, C., 2000, astro-ph/0005269

Hui, L., 1999, ApJ, 519, 9

Jain, B., Seljak, U., 1997, ApJ, 484, 560

Jain, B., Seljak, U., White, S.D.M., 2000, ApJ, 530, 547

Kaiser, N., 1992, ApJ, 388, 272

Kaiser, N., Wilson, G., Luppino, G.A., 2000, astro-ph/0003338

Miralda-Escude, J., 1991, ApJ, 380, 1

Moutarde, F., Alimi, J.-M., Bouchet, F.R., Pellat, R., & Ramani, A. 1991, ApJ, 382, 377

Munshi, D., Coles, P., 2000, MNRAS, 313, 148

Munshi, D., Jain, B., 2000a, astro-ph/9911502

Munshi, D., Jain, B., 2000b, astro-ph/9912330

Peacock, J.A., Dodds, S.J., 1996, MNRAS, 280, L19

Peebles, P.J.E., 1980, The Large-Scale Structure of the Universe (Princeton: Princeton University Press)

Schneider, P., Van Waerbeke, L., Jain, B., Kruse, G., 1998, MNRAS, 296, 873

Scoccimarro, R., Frieman, J., 1999, ApJ, 520, 35

Scoccimarro, R., Couchman, H., 2000, astro-ph/0009427

Valageas, P., 2000, A&A, 356, 771

Van Waerbeke, L., Bernardeau, F., Mellier, Y., 1999, A&A, 342, 15

Van Waerbeke, L., Mellier, Y., Erben, T., Cuillandre, J.C., Bernardeau, F., Maoli, R., Bertin, E., Mc Cracken, H., Le Fèvre, O., Fort, B., Dantel-Fort, M., Jain, B., Schneider, P., 2000, A&A, 358, 30

Villumsen, J.V., 1996, MNRAS, 281, 369

White. W., & Hu, W. 2000, ApJ, 537, 1

Wittman, D.M., Tyson, J.A., Kirkman, D., Dell'Antonio, I., Bernstein, G., 2000, Nature, 405, 143